Biochimica et Biophysica Acta 1837 (2014) 1581–1593

Contents lists available at ScienceDirect

Biochimica et Biophysica Acta

journal homepage: www.elsevier.com/locate/bbabio

eGFP-pHsens as a highly sensitive fluorophore for cellular pH determination by fluorescence lifetime imaging microscopy (FLIM) ☆

Franz-Josef Schmitt [a,*], Bastian Thaa [b], Cornelia Junghans [a], Marco Vitali [a], Michael Veit [b], Thomas Friedrich [a]

[a] Technical University of Berlin, Institute of Chemistry, Sekr. PC 14, Straße des 17. Juni 135, D-10623 Berlin, Germany
[b] Free University of Berlin, Department of Veterinary Medicine, Institute of Virology, Robert-Ostertag-Str. 7-13, D-14163 Berlin, Germany

ARTICLE INFO

Article history:
Received 11 January 2014
Received in revised form 7 April 2014
Accepted 8 April 2014
Available online 14 April 2014

Keywords:
GFP
FLIM
pH determination
M2 proton channel
Xanthophyll cycle
pH-dependent ROS

ABSTRACT

The determination of pH in the cell cytoplasm or in intracellular organelles is of high relevance in cell biology. Also in plant cells, organelle-specific pH monitoring with high spatial precision is an important issue, since e.g. ΔpH across thylakoid membranes is the driving force for ATP synthesis critically regulating photoprotective mechanisms like non-photochemical quenching (NPQ) of chlorophyll (Chl) fluorescence or the xanthophyll cycle. In animal cells, pH determination can serve to monitor proton permeation across membranes and, therefore, to assay the efficiency of drugs against proton-selective transporters or ion channels. In this work, we demonstrate the applicability of the pH-sensitive GFP derivative (eGFP-pHsens, originally termed deGFP4 by Hanson et al. [1]) for pH measurements using fluorescence lifetime imaging microscopy (FLIM) with excellent precision. eGFP-pHsens was either expressed in the cytoplasm or targeted to the mitochondria of Chinese hamster ovary (CHO-K1) cells and applied here for monitoring activity of the M2 proton channel from influenza A virus. It is shown that the M2 protein confers high proton permeability of the plasma membrane upon expression in CHO-K1 cells resulting in rapid and strong changes of the intracellular pH upon pH changes of the extracellular medium. These pH changes are abolished in the presence of amantadine, a specific blocker of the M2 proton channel. These results were obtained using a novel multi-parameter FLIM setup that permits the simultaneous imaging of the fluorescence amplitude ratios and lifetimes of eGFP-pHsens enabling the quick and accurate pH determination with spatial resolution of 500 nm in two color channels with time resolution of below 100 ps. With FLIM, we also demonstrate the simultaneous determination of pH in the cytoplasm and mitochondria showing that the pH in the mitochondrial matrix is slightly higher (around 7.8) than that in the cytoplasm (about 7.0). The results obtained for CHO-K1 cells without M2 channels in comparison to M2-expressing cells show that the pH dynamics is determined by the specific H^+ permeability of the membrane, the buffering of protons in the internal cell lumen and/or an outwardly directed proton pump activity that stabilizes the interior pH at a higher level than the external acidic pH. This article is part of a Special Issue entitled: Photosynthesis Research for Sustainability: Keys to Produce Clean Energy.

1. Introduction

The measurement of pH in the cell cytosol or with high spatial precision in cell organelles localized at specific subcellular structures is of high interest for different applications ranging from molecular cell biology and biomedicine to photosynthesis research. In the latter approach, the activity of photosystem II (PSII) can be efficiently examined by measuring the fluorescence of chlorophyll (Chl) *a*, most frequently in the form of transient fluorescence measurements by recording Chl fluorescence induction curves imaging the transient development of photochemical and nonphotochemical quenchers in dark-adapted samples after excitation by intense light [2–4].

Several other techniques of fluorescence detection are used to analyze PSII activity. Delayed fluorescence (DF) is a suitable indicator to measure the recombination fluorescence response at the reaction centers of PSII that can be monitored as a very weak fluorescence signal with characteristic kinetics [5–7]. Prompt Chl fluorescence is analyzed to obtain the rate constants for charge separation and charge stabilization directly by evaluating time- and wavelength-resolved fluorescence measurements with model-based kinetic analysis [8,9].

Abbreviations: Chl, chlorophyll; CHO, Chinese hamster ovary; DAS, decay-associated spectra; deGFP, dual emission eGFP; eGFP, enhanced green fluorescent protein; FLIM, fluorescence lifetime imaging microscopy; GFP, green fluorescent protein; MA, multi-anode; NPQ, nonphotochemical quenching; PBSeq, phosphate buffered saline-equivalent; PMT, photomultiplier tube; ROS, reactive oxygen species; PS, photosystem; qE, energy-(ΔpH)-dependent NPQ component; RFP, red fluorescent protein; TWCSPC, time- and wavelength-correlated single photon counting; WFMP, wide-field multi-parameter; WOC, water-oxidizing complex; YFP, yellow fluorescent protein

☆ This article is part of a Special Issue entitled: Photosynthesis Research for Sustainability: Keys to Produce Clean Energy.

* Corresponding author at: Sekr. PC 14, Straße des 17. Juni 135, 10623 Berlin, Germany. Tel.: +49 30 314 23511.
E-mail address: schmitt@physik.tu-berlin.de (F.-J. Schmitt).

http://dx.doi.org/10.1016/j.bbabio.2014.04.003
0005-2728/

When electrons are vectorially transferred from the lumen to the stroma across the thylakoid membrane, protons are transferred in the opposite direction. More specifically, when electrons in PSII are transferred from the water-oxidizing complex (WOC) via tyrosine Y_Z to the oxidized primary donor $P680^{+\bullet}$ in the reaction center, protons are released into the lumen [10–12]. Therefore, the highly localized measurement of pH changes and proton release into the thylakoid lumen during the activity of the photosynthetic reaction centers would complement the fluorescence data and help to establish a technical approach for monitoring the principal bioenergetic processes in photosynthesis including proton transfer. Such an approach would be of interest for analyzing the coupling of electron transfer (ET) steps to proton release at the WOC [10–14]. From a more general point of view, the electrochemical gradient for protons (the 'proton-motive force') is the energy source that couples between electron and hydrogen transfer in oxidative as well as photosynthetic phosphorylation according to the chemiosmotic hypothesis devised by Peter D. Mitchell in 1961 [15]. Thus, the proton-motive force, either generated by oxygenic photosynthesis in thylakoid membranes of cyanobacteria or chloroplasts of higher plants, or built-up by the respiratory chain complexes in the inner membrane of mitochondria, ultimately empowers ATP synthesis by F_0F_1-ATPases [16]. In this context, techniques that allow determining $[H^+]$ quantitatively and with high spatial precision in vivo are critical for the investigation of the fundamental bioenergetic processes in plants as well as animal physiology. Moreover, the ΔpH built-up across the thylakoid membrane by the complexes of oxygenic photosynthesis also serves as a mediator for protective mechanisms that safeguard photosynthetic organisms against the harmful impacts of excessive light energy in order to balance between absorption and utilization of light and, in particular, to avoid photooxidative damage. Under extreme light, the excitation energy deposited on Chl molecules cannot completely be fed into the photochemical quenching processes, which results in a rise of Chl fluorescence and increased risk of formation of excited Chl triplet states and subsequent generation of reactive oxygen species (ROS). Therefore, various mechanisms of non-photochemical quenching (NPQ) are triggered (see [17] for review), ranging from the light-induced and pH-dependent xanthophyll cycle [18–21], to activation of the orange carotenoid protein (OCP) in cyanobacteria, to the specific light-harvesting complex stress-related (LHCSR) protein in algae and to the PsbS subunit of PSII in higher plants [22,23], which is an independently evolved member of the LHC protein superfamily acting as a luminal pH sensor [24]. In this context, the large ΔpH across the thylakoid membrane (with acidic luminal pH) that builds up under extreme light due to the limited capacity of the F_0F_1-ATPase system is the most immediate biochemical signal for triggering NPQ mechanisms [17], and it is responsible for the most rapidly responding energy-(ΔpH)-dependent NPQ component (qE) [25,26]. Two processes are initiated by acidic luminal pH: the pH-sensing PsbS protein of plants first undergoes conformational changes [27] and most likely triggers a rearrangement of PSII supercomplexes in grana [25], and then in effect, promotes the induction of NPQ by reducing the semi-crystalline ordering and increasing the fluidity of protein organization in the membrane [28]. Likewise, the LHCSR protein in algae functions as a pH-sensitive site for quenching of excitation energy by a Chl–carotenoid charge transfer mechanism [24]. Second, low lumenal pH triggers the xanthophyll cycle [19] by activating pH-dependent xanthin deepoxidases. In the violaxanthin cycle of plants and green or brown algae, the violaxanthin deepoxidase converts violaxanthin via antheraxanthin to zeaxanthin, whereas diatoms and many eucaryotic algae perform the diadinoxanthin cycle [25]. Xanthin deepoxidases associate with thylakoid membranes at low pH to act on their substrates [25]. Although it is known since many years that zeaxanthin may act as a direct quencher of Chl fluorescence [29], the mechanism by which zeaxanthin deactivates more efficiently than violaxanthin is still not completely understood. All carotenoids with more than ten conjugated C═C bonds have an excited singlet S_1 state low enough to accept energy from excited Chl. However, the S_1 state cannot be populated by one-photon absorption, but it can be reached upon rapid internal conversion from the S_2 state. In vitro determination of the energy levels of the S_1 state of zeaxanthin and violaxanthin showed that both pigments have an S_1 state suitable for direct quenching of excited Chl through singlet–singlet energy transfer. Experimental evidence suggests that violaxanthin is implicated in direct quenching of LHCII, since its particularly short fluorescence lifetime of 10 ps was found in femtosecond transient absorption experiments in intact thylakoids under maximal qE [30]. Recent results emphasize that the switch between the light-harvesting and photoprotective modes of the light-harvesting system is antagonistically operated by zeaxanthin and violaxanthin and that the xanthophyll cycle pool size is critical to optimize the kinetics of NPQ [20]. Furthermore, a common quenching process might underlie the zeaxanthin-dependent as well as the zeaxanthin-independent qE component, most likely based upon a conformational change within the PSII antenna, optimized by LHC subunit interactions and synergistically tuned by external and internally bound xanthophylls [21]. Altogether, the pH-dependent qE component of NPQ and the xanthophyll cycles highlight the importance of organelle-specific pH quantification techniques with the help of genetically targetable GFP sensor proteins.

Determination of the local pH plays also an important role in imaging ROS production and signaling. The nature of ROS generated during illumination of photosynthetic organisms strongly depends on the pH mainly in the thylakoid lumen, and, vice versa, the generation of ROS determines the local pH. The nature of ROS leads to oxidative damage of cellular structures and triggers delay or acceleration of the repair of damaged cell structures. In addition, ROS also act as important signaling molecules with regulatory functions. ROS were found to play a key role in the transduction of intracellular signals and in the control of gene expression and the activity of antioxidant systems. It is therefore of highest relevance to study the interaction of ROS in dependency of the local pH [31–35]. One prominent species of ROS formed at PSI is the superoxide radical ($O_2^{-\bullet}$), which cannot pass the membrane due to its charge. Due to its pK_a of 4.8, $O_2^{-\bullet}$ can get protonated at sufficiently acidic pH and pass membranes in the form of hydroxyl radicals ($HO^\bullet$), which is essential for signaling. $HO^\bullet$ is the most reactive ROS known to biology with a midpoint potential of +2.33 V at pH 7. Since the luminal pH can reach values down to 4.5 [36], while other publications report values between 5.0 and 5.5 [37], the dynamics of the $O_2^{-\bullet}/HO^\bullet$ system is still a matter of debate that might be elucidated with techniques for highly localized pH determination [35].

Genetically encoded fluorescence proteins based on or derived from the green fluorescent protein (GFP) and its spectral variants from various species allow for the selective labeling of proteins and their investigation in vivo [38–41]. Wild-type GFP from *Aequorea victoria* shows a bimodal absorption spectrum with a maximum at 395 nm and a shoulder at 470 nm. The 395/470 nm absorbance ratio is about 2.0 at neutral pH and changes in a pH-dependent manner from 6.5 to 0.42 at pH 12.2 [42]. The two maxima relate to the protonated and deprotonated states of Tyr-66 in the chromophore triad [43,44] indicating that GFP can assume two alternative conformations: first with the protonated chromophore, which is excited at 395 nm, and second with a deprotonated chromophore with excitation at 475 nm [43]. It was shown that the S65T mutation in GFP simplifies the excitation spectrum to a single peak at 488 nm of enhanced amplitude [45], which no longer shows signs of conformational/protonation state isomers. Although the shape of the fluorescence excitation and emission spectra did not change with pH, the intensities decreased continuously with decreasing pH down to 50% of maximal intensity at a pH of 6.0 [46], but, notably, no change in the fluorescence lifetime was found in the pH range from 5 to 10 [46].

It is assumed that chromophore protonation/deprotonation in GFP relies on a hydrogen bond network around the chromophore that allows for rapid and directed proton transfer along the protein structure from the chromophore environment to the surrounding solvent [44,

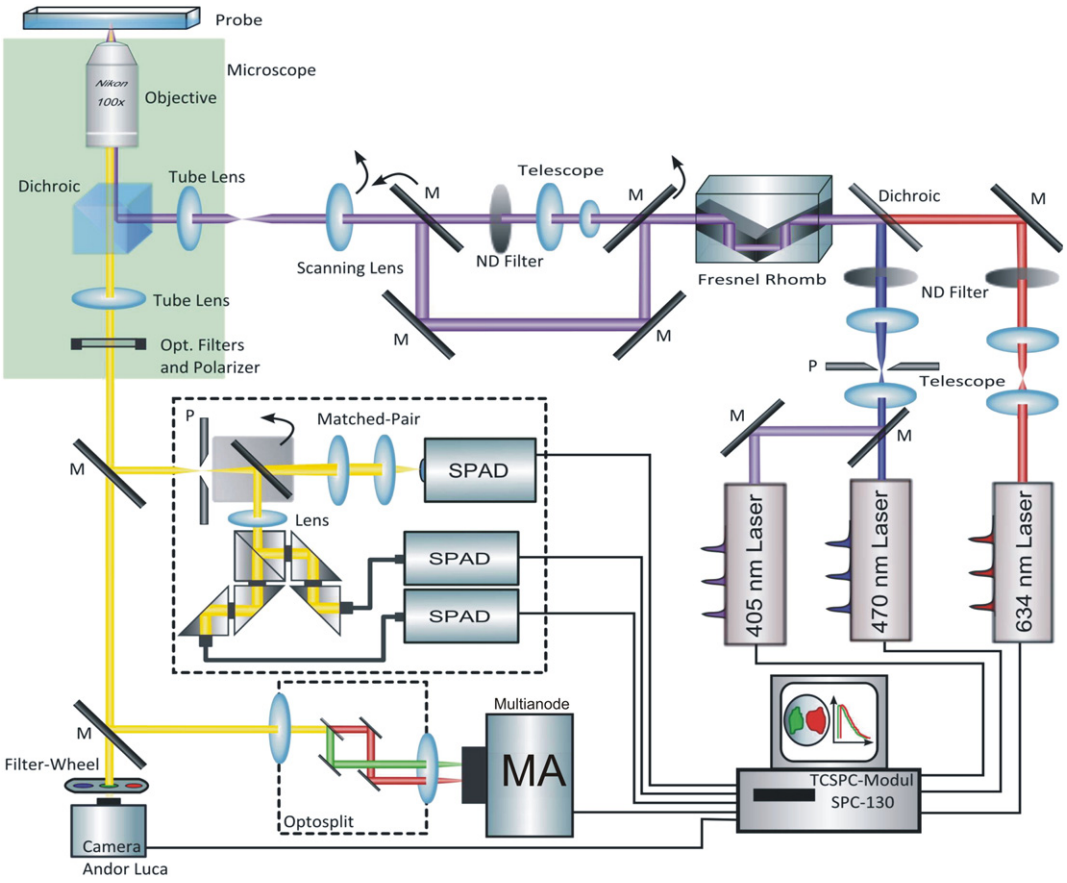

Fig. 1. Scheme of the multi-parameter FLIM setup based Nikon TI Eclipse wide-field fluorescence microscope (for details see text).

47]. Since these processes strongly influence the optical properties and lead to a profound pH dependence, extensive efforts have been undertaken to tailor the fluorescence properties of GFP for sensing applications by mutagenesis approaches.

However, a single emission band from GFP cannot easily be employed for pH sensing since the expression level varies strongly making it impossible to discriminate the (variant) specific GFP fluorescence signal from (also variant) cellular autofluorescence. The pH-dependent lifetime changes of GFP are also small impeding the possibility to discriminate the GFP component from the complex contributions of cellular autofluorescence. Thus, one optimization strategy might follow the mechanism of established exogenous fluorescence probes like fluorescein-isothiocyanate (FITC) or carboxy-SNAFL2, which can be used for ratiometric pH measurements [1]. The problem with these substances is the rather unspecific cell penetration in vivo, while GFP could directly be targeted or fused to specific target proteins for precise sub-cellular localization and analysis in vivo. To exploit the potential of GFP for sensing the chemical environment around the molecule, extensive studies have been undertaken to develop GFP-based in vivo pH sensors by mutational approaches. Such genetic optimization studies, aimed at augmenting the pH dependence of fluorescence that is already present in GFP wildtype [42,48,49], resulted in the development of the class of 'ratiometric' and 'ecliptic' GFP-based pH sensors termed pHlourins [43]. Also, the "dual emission" GFPs (deGFPs) belong to the ratiometric sensor class that switch from a green (λ_{max} ~ 515 nm) to a blue form (λ_{max} ~ 460 nm) upon acidification (with decreasing pH) [1], which has been shown to permit ratiometric pH measurements in vivo [43,46,50–52]. The ratiometric comparison of two different emission bands diminishes, but not completely abolishes the problem of discrimination from the autofluorescence background, but at least, the pH determination becomes rather independent from the expression level.

In particular, Hanson et al. [1] investigated two candidates of the deGFP class, the variants deGFP1 (carrying mutations S65T/H148G/T203C, pK_a ~ 8.0) and deGFP4 (carrying mutations S65T/C48S/H148C/T203C, pK_a ~ 7.3). At high pH, an excited state proton transfer (ESPT) was suggested as an underlying mechanism which is blocked at low pH. At high pH rapid ESPT from the neutral chromophore to the solvent is possible. The negatively charged chromophore shifts the energetic level of the first electronically excited state to lower energies and the fluorescence appears green. Due to a distorted hydrogen bond network at low pH this ESPT interrupts and the fluorescence appears blue [1].

Hanson et al. successfully employed deGFPs in different mammalian cell lines (e.g. CHO-K1). However, the broad unspecific emission of autofluorescence also complicates ratiometric techniques in cells. In the case of large cell-to-cell variability of the GFP expression level and/or varying autofluorescence, ratiometric detection techniques relying on the exclusive measurement of fluorescence amplitudes are prone to profound systematic errors. This generally requires rigorous sets of controls to cope with the variances of biological matter. An alternative would be to identify a different parameter of the deGFP fluorescence, which allows it to discriminate from other (auto)fluorescence sources. Such a parameter could be the fluorescence lifetime. Since the deGFP fluorescence lifetime is characteristic, one can quantify the presence of deGFP and determine the contribution of the background signal from a single decay curve at a fixed wavelength.

Besides the pH value in the cytoplasmic lumen, various other reaction areas such as cell organelles underlie strict pH regulation, for example the endoplasmatic reticulum, or endocytotic vesicles in the kidney or at synapses in the central nervous system, or phagocytotic vesicles during the immune response. In certain cell organelles, for example inside the interior mitochondrial membrane, the actively regulated proton gradient is essential for the primary supply of the cell with ATP [53–56]. For that purpose, cells contain a huge number of proton

transporters or proton selective ion channels in the multitude of cellular membranes. Other examples of proton transport are the proton-potassium-ATPase of the stomach mucous membrane (gastric H^+/K^+-ATPase), which is responsible for the acidification of the stomach lumen [57,58], and the voltage-gated proton channel Hv1, which plays an important role in phagosomes of immune cells and the motility of male sperm [59].

Even some viruses exploit proton-transporting systems for their infection or reproduction cycle. It is known that influenza viruses encode a proton-selective ion channel in their genome (since this is derived from the influenza A virus M2 protein, it is called the 'M2 channel'), which is also present in the viral envelope, and they induce its expression in infected cells. The M2 channel is necessary for the early and in some strains also for the late phase of the replication cycle of the influenza A virus and especially allows for the release of viral ribo-nucleoprotein complexes upon acidification of the virion core that occurs after receptor-mediated endocytosis of viral particles and subsequent endosomal acidification [60–62].

Therefore, proton-transporting membrane proteins represent important pharmacological targets. An application of in vivo pH measurements with deGFPs aiming to determine the activity of the M2 channel would demonstrate the power of fluorescence lifetime measurements suitable for pharmaceutical studies. For treatment of infections with influenza A viruses in Germany only two drugs, Tamiflu® (Roche) and Relenza® (GlaxoSmithKline) are permitted, which both are directed against the same target protein, the viral neuraminidase.

Another antiviral drug, amantadine, specifically blocks the M2 channel, but this substance is rarely used for human therapy due to its severe side effects and the rapid emergence of resistant virus mutants [62]. By a reliable, target-oriented, and fast-responding method for analyzing the activity of viral proton channels, significant progress in pharmacological research could be achieved.

The functionality of the M2 channel has so far been tested only with laborious and complex biochemical and electrophysiological methods. Ion-selective electrodes can only be used in electrophysiological experiments on single cells, but this method is not suitable for high-throughput screening due to the extensive time requirements and the need for highly specialized personnel. For example, the M2 protein has to be expressed in the plasma membrane of oocytes of the clawed frog *Xenopus laevis* (or in other cells that can be handled with electrophysiology) and investigated using the two-electrode voltage-clamp and patch-clamp technique [63–65].

Other approaches use purified M2 protein reconstituted into artificial lipid membranes (liposomes), which separate two electrically isolated compartments from each other and thus allow for the measurement of the ion flow through the membrane. Besides the problem to obtain a preferred orientation of the M2 protein in the reconstituted membranes, also these methods require considerable experimental skill and are only suitable for small numbers of substances to be tested.

To measure the activity of the M2 proton channel in eukaryotic cells in vivo, a fluorescence-based system that could be used by the pharmaceutical industry for high-throughput screening in drug research would be advantageous. The use of fluorophores based on functionalized fluorescence proteins in general offers the most promising tool because it also permits the application of recently developed advanced techniques of ultrahigh time- and space-resolved fluorescence microscopy for in vivo studies [66].

In the study presented here, it is shown that the fluorescence lifetime of eGFP-pHsens is a superior parameter for the quantitative analysis of pH in cells after excitation of eGFP-pHsens at 405 nm allowing the simultaneous ratiometric (460 nm vs. 520 nm band) and kinetic analysis (at 520 nm) of the fluorescence properties. Such time-resolved spectroscopy of the pH sensitive emission has been previously reported for the pH-sensitive exogenous fluorescence dye carboxy-SNAFL2 [67]. An application of complementary studies employing time-resolved measurements and spectrally resolved fluorescence intensity with a multiparameter fluorescence setup was previously published for applications in studying FRET efficiency [68].

2. Materials and methods

2.1. cDNA constructs and mammalian cell expression

Mutations C48S, H148C and T203C were introduced into the eGFP cDNA within the pEGFP-N1 vector (Life Technologies) using the QuikChange Site-Directed Mutagenesis Kit (Stratagene) to obtain deGFP4, or eGFP-pHsens, as denoted in this work. The cDNA of the M2 protein from influenza A virus (see GenBank acc. no. CY088486, 97 amino acid sequence: MSLLTEVETPTRNGWECRCSDSSDPLVIAASIIGILHL ILWILDRLFFKCIYRRLKYGLKRGPSTEGVPESMREEYRQEQQSAVDVDDGHF VNIELE) was first subcloned in-frame into the pEGFP-N1 vector to obtain an M2-eGFP fusion protein. Subsequently, the eGFP cDNA in this construct was replaced by the cDNA of the red fluorescent protein TagRFP-T (from TagRFP-T cDNA in vector pcDNA3, a kind gift of W. Zuschratter, IfN Magdeburg) by recombinant PCR, resulting in construct M2-TagRFP. For targeting eGFP-pHsens to mitochondria, the eGFP-pHsens cDNA was subcloned into the pHyper-mito vector (Evrogen), which carries the first 30 N-terminal amino acids of the subunit VIII of human cytochrome C oxidase as mitochondrial targeting sequence, by exchanging the cDNA of the hydrogen peroxide sensor 'Hyper' [41] by the cDNA of eGFP-pHsens using recombinant PCR. All PCR-derived fragments were verified by sequencing (Eurofins MWG Operon). CHO-K1 cells were transfected with cDNA of either eGFP-pHsens only or together with M2-TagRFP cDNA in a 1:1 mixture using Lipofectamine 2000 (Life Technologies) as a transfection reagent according to the manufacturer's instructions. Cells were used 24–48 h after transfection.

2.2. Expression and purification of eGFP-pHsens from Escherichia coli

For expression of eGFP-pHsens in *E. coli*, the cDNA was subcloned by *Bam*HI/*Not*I digestion into a modified pQE81L-Amp vector (Qiagen) harboring an additional *Not*I restriction site. This procedure results in a protein with an N-terminal 6xHis tag.

After transformation of the plasmid into NEB turbo cells (New England Biolabs), liquid cultures were grown to OD 0.6 and expression was induced by adding 100 μM IPTG. After growing cells at room temperature for 48 h, cells were harvested by centrifugation yielding deeply green-colored pellets indicating expression of eGFP-pHsens. Cell pellets were resuspended in phosphate buffer and lysed by two passages through a French press (18,000 psi). After removal of the cell debris by centrifugation (24,000 ×*g*, 4 °C), the clarified supernatant was purified on a Ni^{2+}-Sepharose column (GE Healthcare) according to the manufacturer's manual (20 mM Imidazol was supplemented to the supernatant, as recommended). The fractions with the highest absorbance at 470 nm were pooled and dialyzed against 50 mM Tris/HCl, 300 mM NaCl, and 5 mM EDTA (pH 7.8).

2.3. pH calibration measurements with the purified protein and in living cells

For measuring the fluorescence lifetime response of eGFP-pHsens in vitro, the purified protein was suspended in PBS-equivalent (PBSeq) solutions (137 mM NaCl, 2.7 mM KCl, 5 mM Tris, 5 mM HEPES, 5 mM MES) titrated to varying pH values and the fluorescence lifetime was determined by FLIM in cells or by time-resolved fluorescence spectroscopy on the purified protein in a cuvette.

For pH measurements in mammalian cells, CHO-K1 cells transfected with eGFP-pHsens cDNA were transferred into PBSeq solutions (vide supra) with varying pH ranging from pH 5.0 to pH 8.0. Nigericin and monensin (both from Sigma-Aldrich) were added to PBSeq solutions at a final concentration of 5 μM for both ionophores. Cells were incubated with the ionophore-containing PBSeq solution for

30 min to allow for the relaxation of the cytosolic pH to the external pH. For dynamic experiments, the microscopy dish containing CHO-K1 cells at fixed pH was washed with fresh PBSeq directly under the microscope to change the pH of the medium.

2.4. Fluorescence lifetime imaging microscopy (FLIM)

The technique of wide-field multi-parameter (WFMP) FLIM was developed and applied for continuous and sensitive monitoring of living cells. The WFMP-FLIM setup (see Fig. 2, [68]) is based on a Nikon TI Eclipse wide-field fluorescence microscope equipped with 100× (N.A. 1.4) objective. Excitation was performed with a 405 nm picosecond laser diode driven at 20 MHz (LDH-405, Picoquant, Berlin). The pulse train was focused on the back focal plane of the objective to achieve a uniform illumination of the whole field of view. A dichroic cube (488-DXCR—Cairn Research Limited, Faversham, UK) and an emission filter (405 nm Notch, AHF Analysentechnik, Tübingen) were used to remove the stray light of the laser from the fluorescence signal. Three band pass filters (460/40, 520/35 and 605/55 AHF Analysentechnik AG, Tübingen, Germany) were used to select the desired spectral channels for the blue emission band of eGFP-pHsens, the green emission band of eGFP-pHsens and the emission band of TagRFP-T, respectively. Images were taken with an electron-multiplying CCD (EMCCD), Andor Luca (Andor Technologies, UK). For FLIM the images were projected on a newly developed actively cooled time- and space-resolving multi-anode (MA) photomultiplier with the highest throughput (up to 10^6 photons/s) and lowest noise (<10 photons/s) for ultrasensitive wide-field observations with high time and space resolution (Leibniz Institute for Neurobiology, Magdeburg, Germany). The setup allows for fast switching between all excitation and detection modes. It is equipped with several fully automated optical add-ons to switch between different operation modes (see Fig. 2, [68]).

The MA detector is equipped with a double-stage microchannel plate photomultiplier (MCP-PMT) and several separate anode elements equipped with a novel MA-Proximity-MCP-PMT-measurement head. These anode elements represent a charge division pattern comprising four planar and electrically isolated electrodes and a fifth cylindrical one surrounding the planar structure. An incident photon releasing an electron from the photocathode leads to the amplification of the electron to an avalanche along the MCP-PMT stack. The impinging electron avalanche on the sectorized anode is registered. As the anode elements are divided into several electrodes each position of the initially registered photon on the photocathode leads to a certain spatial distribution of the charges from the avalanche on the anode sectors. The combination of the measured charge on all anode elements therefore allows determining the position of the incident photon by the charge division technique [68].

The average lifetime of the fluorescence decay for spatially resolved FLIM pictures is calculated with the program QA analysis (Europhoton, Berlin, Germany) and plotted in color representation of the average fluorescence time to show the spatial dependency of the fluorescence decay time (FLIM pictures).

2.5. Time- and wavelength-correlated single photon counting (TWCSPC)

TWCSPC measurements were performed with a similar setup as described in [8,68,69] employing a Hamamatsu R5900 16-channel MA photomultiplier tube (PMT) with 16 separate output (anode) elements and a common cathode and dynode system (PML-16C, Becker&Hickl, Berlin, Germany). The polychromator was equipped with a 300 grooves/mm grating resulting in a spectral bandwidth of the PML-16C of about 12.5 nm/channel. A 405 nm pulsed laser diode (LDH-405, Picoquant, Berlin) was used for excitation. For further details, see [70].

2.6. Decay-associated spectra (DAS)

The fluorescence decay was analyzed employing a Levenberg–Marquardt algorithm for the minimization of the reduced χ_r^2 after iterative reconvolution with the instrumental response function (IRF). The value of χ_r^2 depends on a parameter set $(p_1,\ldots,p_n)$ of the chosen continuous fit function $A(t,\lambda,p_1,\ldots,p_n)$ for the temporally discrete fluorescence points $F(t_\nu,\lambda)$.

The function χ_r^2 is evaluated in each time t_ν channel ($\nu = 1, \ldots, 4096$) after convolution of the determined fit function $A(t,\lambda,p_1,\ldots,p_n)$ with the IRF and averaged over all time channels:

$$\chi_r^2(p_1,\ldots,p_n,\lambda) = \sum_{\nu=1}^{4096} \frac{1}{\sqrt{F(t_\nu,\lambda)}} \left(\frac{F(t_\nu,\lambda) - A(t_\nu,\lambda,p_1,\ldots,p_n)}{\sqrt{F(t_\nu,\lambda)}} \right)^2. \quad (1)$$

$A(t,\lambda,p_1,\ldots,p_n)$ was chosen as a biexponential decay function

$$A(t,\lambda) = \sum_{j=1}^{2} a_j(\lambda) e^{-t/\tau_j}, \quad (2)$$

with the parameters $a_j(\lambda)$ and τ_j denoting wavelength dependent amplitude and time constant of the jth exponential decay component for two components ($n = 2$), respectively. The biexponential fits of all decay curves measured in one time- and wavelength resolved

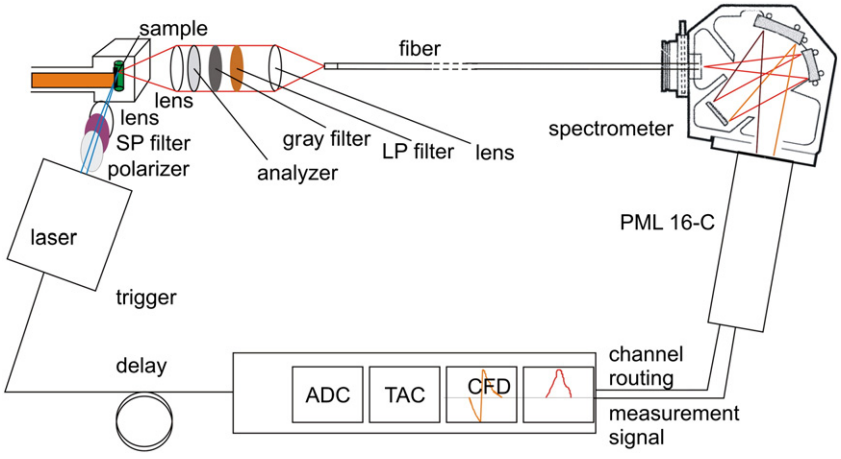

Fig. 2. Measurement setup used for TWCSPC with optical path shown in blue for excitation from the laser source via optional polarizer and short pass (SP) filter. The fluorescence light (red) is monitored via analyzer (optional), gray filter and long pass (LP) filter into the spectrometer system connected with the MA PMT system PML-16C. The PMT signal is processed via constant fraction discriminator (CFD), time-to-amplitude converter (TAC) and analog-to-digital converter (ADC) (see [8,68]).

fluorescence spectrum were performed as global fits with common values of lifetimes τ_j (linked parameters) for all decay curves and wavelength-dependent pre-exponential factors $a_j(\lambda)$ (non-linked parameters). The result of this analysis is usually plotted as a graph of $a_j(\lambda)$ for all wavelength independent lifetimes τ_j representing the so-called DAS, thus revealing the energetic position of individual decay components.

The quality of the fit was judged by the value of χ_r^2.

For this calculation the software Globals Unlimited® (University of Illinois, Urbana, USA) was used. It was found that a sufficient quality of the fit could be achieved for the fluorescence decay curves of eGFP-pHsens when the decay curves were fit with $n = 2$ decay components ($\chi_r^2 = 1.4$). No significant improvement was obtained with $n > 2$ decay components.

3. Results

The normalized fluorescence decay curves of eGFP-pHsens at 520 nm at different pH values, measured in CHO-K1 cells that had been permeabilized by monensin and nigericin to achieve effective pH equilibration of the intracellular space, are shown in Fig. 3, (panel a) in comparison to a typical autofluorescence decay of untransfected cells excited with 405 nm laser light (gray curve, panel a). The decay curves were monitored at 520 nm with the FLIM setup as described in Materials and methods. Fig. 3, (panel b) shows the same situation for the purified eGFP-pHsens in PBSeq at different pH values measured with the PML-16C (see Materials and methods). The fluorescence decay of eGFP-pHsens is determined by a slow decay component (2.6–2.7 ns), which dominates the fluorescence decay at pH 8 (magenta curve). The contribution of a rather fast decay component (100–200 ps) is rising in amplitude with reducing pH (black curve for pH 5.0). The complex decay of the autofluorescence (gray curve) which exhibits a broad lifetime distribution including species with very long fluorescence lifetime differs clearly from the characteristic kinetics of eGFP-pHsens. It is important to note that the autofluorescence curve in Fig. 3a was scaled up upon normalization. The absolute amplitude of the autofluorescence signal compared to the eGFP-pHsens signal depends strongly on the expression level of eGFP-pHsens and the applied excitation wavelength. It can vary from less than 1% up to fluorescence signals that are higher in amplitude than the eGFP-pHsens signal in weakly expressing cells.

The clear separation of the different decay curves at different pH values for CHO-K1 cells expressing eGFP-pHsens (Fig. 3 a) shows that the fluorescence lifetime of eGFP-pHsens is a sensitive indicator for the local pH in the range of pH 5 to pH 8. In this manner, eGFP-pHsens is a highly suitable pH monitor for the evaluation of the pH from the fluorescence lifetime in one wavelength section at 520 nm only. In comparison, the fluorescence decay curves of wild-type eGFP (Fig. 3, panel c) expressed in CHO-K1 cells measured at 520 nm emission wavelength are shown. The pH dependency is much less pronounced for eGFP and shows a clear change of the fluorescence lifetime between pH 6.5 and 7 only. At pH below 6.5 no further acceleration of the decay kinetics was observed.

The pH dependency of the fluorescence lifetime of a typical exogenous dye used for ratiometric measurements like FITC in PBSeq (Fig. 3, panel d) also is less suitable for measuring the pH, since there is no remarkable change of the distribution of two clearly distinguishable lifetimes as observed for eGFP-pHsens (Fig. 3, panels a and b). While in eGFP-pHsens the contribution of the fast component (100–200 ps) rises strongly upon acidification and the amplitude of this fast component in contrast to the 2.6–2.7 ns component can be evaluated, such a behavior is not observed in FITC (Fig. 3d). In FITC, the amplitude of the fast component (1.3 ns at pH 5) in relation to the slow component (2.7 ns at pH 5) is rather stable when the pH changes, but the lifetime itself changes with pH reaching 1.7 ns (fast component) and 3.7 ns (slow component) at pH 8 (data not shown). In fact, such a behavior is less suitable for monitoring of pH via the fluorescence lifetime, since also the autofluorescence shows a broad distribution of fluorescence lifetimes and varies locally. Therefore, the error bar of the pH determination by measurement of a single fluorescence decay curve of FITC is larger in comparison to eGFP-pHsens (data not shown).

The high count rate, which can be achieved with the novel MA detector (IfN Magdeburg), allows to achieve a S/N ratio of > 100 for the spatially

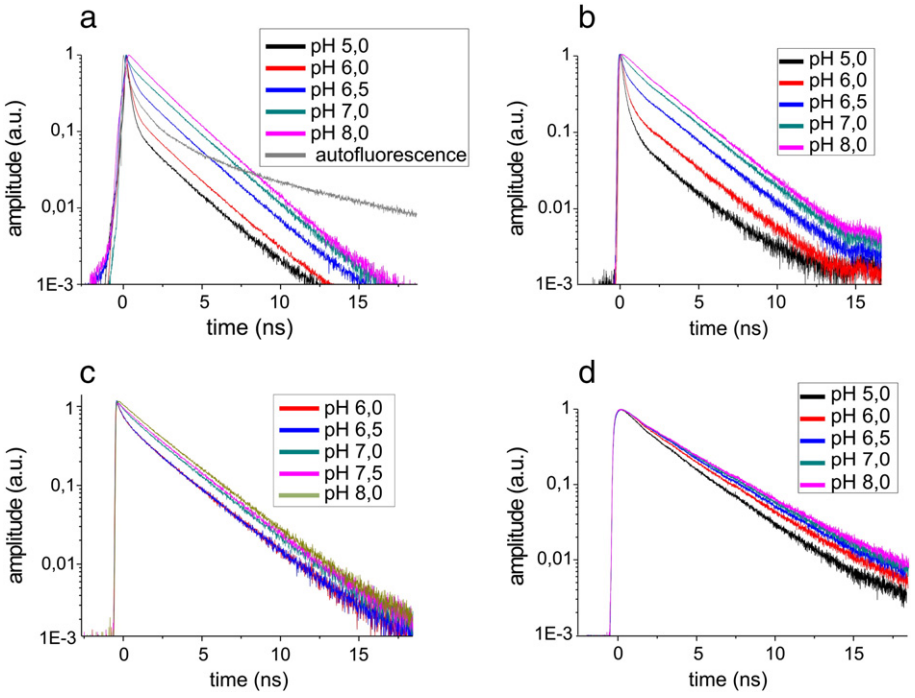

Fig. 3. Fluorescence decay curves of eGFP-pHsens in CHO-K1 cells (panel a) and in solution (PBSeq, panel b) at 520 nm. Wild type eGFP (panel c) expressed in CHO cells monitored at 520 nm and FITC in solution (PBSeq., panel d) in dependency of the pH. The measurements in living cells were performed in the multiparameter FLIM setup (Fig. 1) after excitation at 405 nm at different pH. The measurements in PBSeq were done in solution (PML-16C, Fig. 2). Signals were normalized to the peak amplitude.

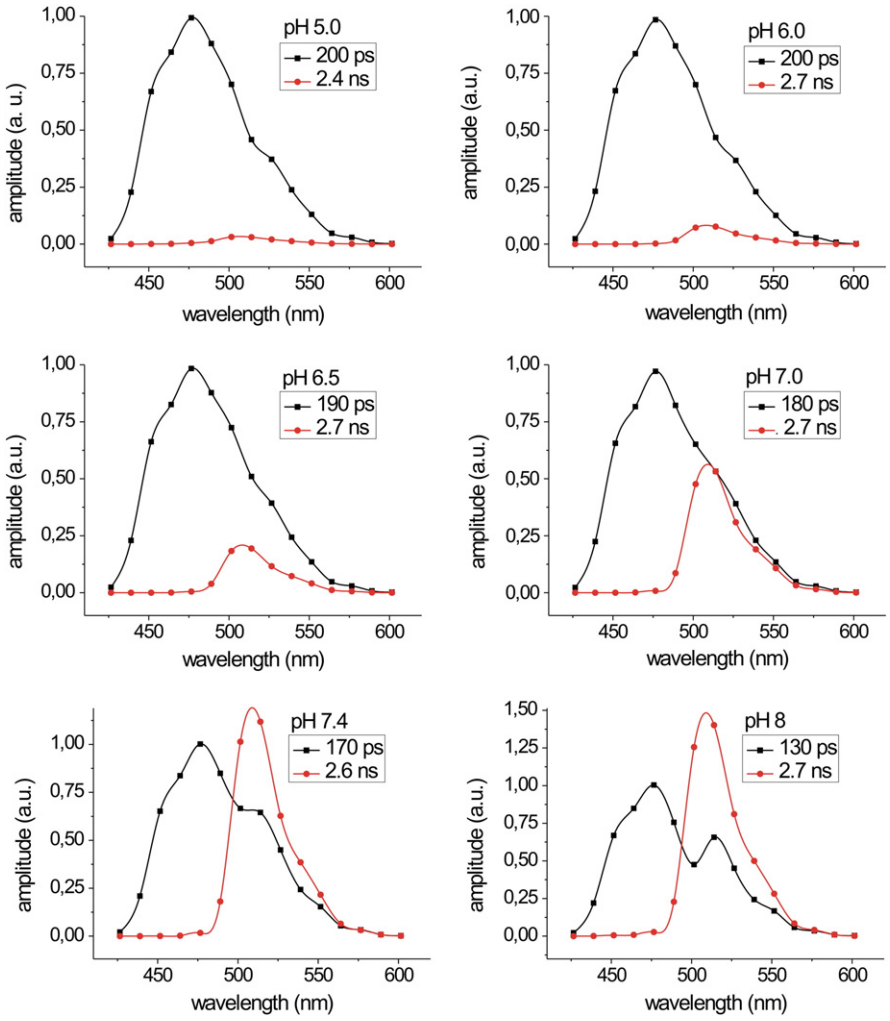

Fig. 4. DAS of eGFP-pHsens after excitation at 405 nm and subsequent global fit with two exponential components of the fluorescence decay data in the range between 426 and 613 nm. The DAS for pH ranging from pH = 5.0 to pH = 8.0 are shown. The amplitudes of the two exponential components are shown in black (130–200 ps) and red (2.4–2.7 ns). The DAS are normalized to the maximum of the 130–200 ps component. The TWCSPC data was collected in 16 wavelength channels with omission of the first channel due to low S/N ratio.

integrated fluorescence decay during 1 s of measurement time, since more than 10,000 photons are collected in the fluorescence maximum. A big advantage is the independency of the pH determination from count rate and S/N ratio by analyzing the relative contribution of the fast (100–200 ps) component in comparison to the slow (2.6–2.7 ns) component. However, it has to be mentioned that the exact time constant and the amplitude distribution of the fast and the slow component slightly depend on the environment of the eGFP-pHsens and differ systematically between solutions of the purified protein and protein expressed in CHO-K1. Further deviation in other host organisms or different environments/status of the protein cannot be excluded. If it can be assumed that ionophores like nigericin and monensin guarantee that the pH in cells equilibrates with the environment which is visible well comparing Fig. 3 (panel a, eGFP-pHsens in CHO-K1 cells) and Fig. 3 (panel b, eGFP-pHsens in PBSeq) the calibration directly in the system of interest is recommended by setting the host onto a specified pH after expressing eGFP-pHsens and registering the lifetime values and amplitude distribution. This calibration has to be done for a specific analysis of the local pH in the same organism under constant conditions for the protein expression. In other cases (if the adaption of the pH after adding ionophores is unknown) eGFP-pHsens in PBSeq solution can be used for calibration.

To obtain a clear picture of the behavior of the fluorescence dynamics of eGFP-pHsens, DAS were calculated from TWCSPC data to elucidate

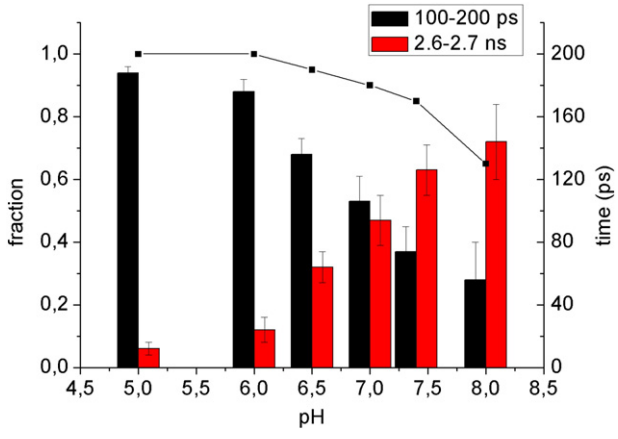

Fig. 5. Relative contributions (relative fraction, left side) and lifetimes (exact value of the 100–200 ps component shown as black squares, scaling at the right side) of both components of a biexponential fit of the fluorescence emission from eGFP-pHsens at 520 nm after excitation with 405 nm laser light at different pH varying from pH = 5.0 to pH = 8.0. The black columns denote the 100–200 ps component, and the red columns denote the 2.6–2.7 ns component. The black squares and the solid line (right axis) show the time constant of the fast component.

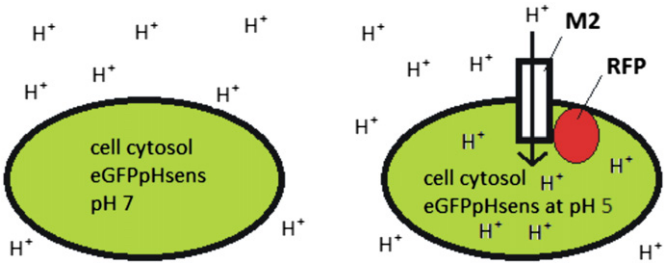

Fig. 6. Left side: Cells expressing the eGFP-pHsens protein only, without the M2 channel and right side: Cells expressing M2 channels as TagRFP-M2 fusion protein together with eGFP-pHsens in the cytoplasm.

the contribution of different fluorescent states in eGFP-pHsens to the overall fluorescence signal. The DAS of eGFP-pHsens in PBSeq buffer at varying pH values after excitation at 405 nm shown in Fig. 4 reveal that at low pH, the fluorescence decay occurs fast with a typical time constant of around 200 ps that shows a fluorescence maximum at about 470 nm, which is in agreement with [1]. The fluorescence spectrum is untypical for the emission of GFP and shows contributions in the blue (460 nm) and red (480 nm) of the main peak as well as a shoulder at 520 nm indicating that different substates are involved in the blue emission upon excitation at 405 nm (see black squares in Fig. 4). At higher pH, when the H-bond network in eGFP-pHsens resembles the natural WT GFP structure, the typical GFP fluorescence spectrum rises with main emission found at 520 nm and the typical phonon sideband at 540–550 nm (red circles in Fig. 4). At pH 8, the fluorescence decay is dominated by the 2.7 ns component. In addition, a significant shift of the time constant of the fast component from 200 ps (pH 5) to 130 ps (pH 8) is visible.

Fig. 5 demonstrates the amplitude distribution of the wavelength-dependent amplitude $a_j(\lambda)$ evaluated at 520 nm for both exponential decay components determined from the data fit after averaging six measurements on two different samples. In addition, the change of the lifetime of the fast component is shown in Fig. 5 at the scaling at the right side (black squares). The confidence interval displays the resulting standard deviation for a single experiment. The dominating component with a typical lifetime of 2.7 ns at pH 8 corresponds to the natural decay time of eGFP displaying the expected GFP spectrum at higher pH (see Fig. 4). At acidic pH, the amount of a rapid decay component with a lifetime of 100–200 ps increases until a ratio of 20:1 with respect to the slow component is reached at pH 5.0. The ratio of both fluorescence components (2.7 ns and 130–200 ps) can be used as a ruler for the local pH in the environment of the fluorescence proteins after measuring one decay curve at 520 nm. In the sensitive regime of the chromophore between pH 5.0 and pH 7.0 an accuracy of 0.3 in determining the local pH can be achieved from a single measurement at 520 nm without background correction and autofluorescence subtraction.

An application for fast and automated measurements of the local pH in cells would for example be the proton exchange via viral proteins like the M2 proton channel of the influenza A virus and the test of the effect of antiviral drugs like amantadine. Amantadine binds to the proton channels formed from M2 proteins and blocks the influx of protons. To test the efficiency of such compounds, the cellular pH change or local change of the pH in endosomes can be analyzed by FLIM of cells expressing eGFP-pHsens as depicted in Fig. 6 as concept for a screening assay. The utilization of a TagRFP-M2 fusion protein allows controlling the expression level and localization of the M2 channel protein. For basic medical research, an assay as depicted in Fig. 6 would also be suitable to select for virus mutants in infected cells via fluorescence-activated cell sorting (FACS) to identify cells infected with viruses, whose M2 channels are insensitive to amantadine. This would allow rapid development of new antiviral drugs, with lower susceptibility to mutational resistance.

Fig. 7 presents two CHO-K1 cells transfected with eGFP-pHsens (shown in green) in overlay with the brightfield EMCCD image (left panel). The CHO-K1 cells were cotransfected with a fusion protein of the M2 proton channel from influenza A virus with TagRFP-T (M2-TagRFP) shown in red (middle panel). eGFP-pHsens is excited with 405 nm pulsed diode laser radiation, while TagRFP-T is excited with light at 530 nm (filter 530/25, AHF Analysentechnik, Tübingen) from a mercury arc lamp. Both proteins (M2-TagRFP and eGFP-pHsens) are registered subsequently in two separate color channels with a filter wheel. The right panel of Fig. 7 shows an overlay of the distribution of eGFP-pHsens and M2-TagRFP.

The same cells shown in Fig. 7 were monitored with the single-photon-counting MA detector (see Fig. 8) to analyze the fluorescence decay time. The results of such a study of cells, in which the extracellular pH was changed from 7.4 to 5 are presented in Fig. 8. The color bar is correlated with the average lifetime $\overline{\tau}$ of the eGFP-pHsens. The average fluorescence decay times shown as color-coded FLIM pictures for the spatially resolved fluorescence lifetime after acidification of the external medium (Fig. 8) indicate how the intracellular pH of two cells expressing M2 ion channels changes with time. While directly after acidification ("0 min") the pH was determined to be 7.2 by comparing the observed lifetime distribution with the calibration data shown in Fig. 5, a final value of about pH 5.5 is reached after 12 min (see Fig. 8).

Fig. 9 shows a different situation, in which two cells express eGFP-pHsens, but only one of them expresses the M2 channel, which illustrates the differences in kinetics of the internal pH change after acidification of the external medium depending on the presence or absence of the M2 channel. In the middle panel of Fig. 9 two cells (green) that express eGFP-pHsens similarly can be seen. As it was schematically depicted in Fig. 6, only one of these cells also expresses the M2-TagRFP

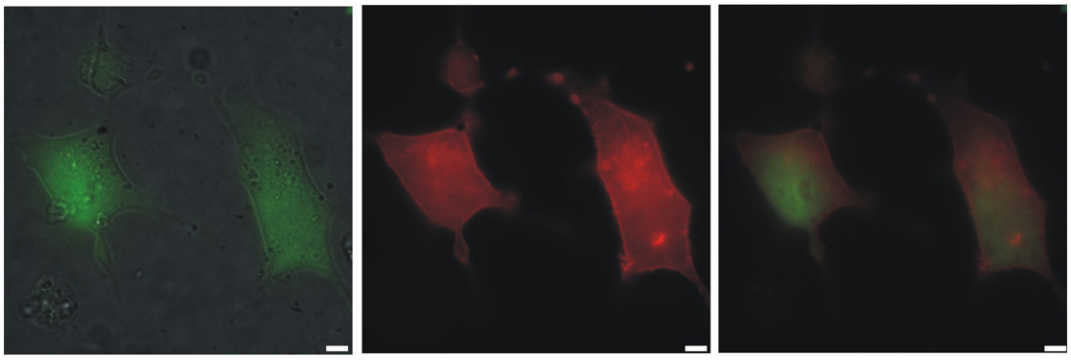

Fig. 7. CHO-K1 cells co-transfected with the pH-sensitive eGFP-pHsens shown in green (left panel) in overlay with the brightfield EMCCD image, and the fusion protein of the influenza virus M2 proton channel with TagRFP-T shown in red (middle panel). The overlay of both fluorescence pictures is shown in the right panel. Scale bar: 5 μm.

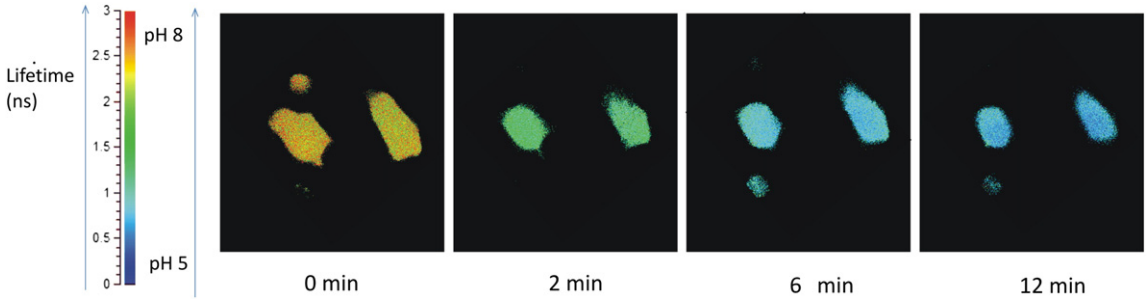

Fig. 8. FLIM data of the cells shown in Fig. 7 after acidification of the external medium. Both cells were cotransfected with eGFP-pHsens and TagRFP-M2.

fusion protein due to the stochastic nature of the transfection procedure (red color in left panel). The plasma membrane localization of the M2 protein is clearly visible in the red detection channel.

After changing the external pH, the cell expressing the M2 proton channel changes its cytoplasmic pH much faster than the cell without M2 channels, as depicted in Fig. 10. The left panel in Fig. 10 depicts a situation in which both cells had been exposed and equilibrated to an external pH of 5.5. From the color representation of the fluorescence lifetime, it is apparent that the cell expressing M2 starts from a far more acidic internal pH than the cell that does not express M2, which still remained at above pH 6.0 even after 20 min of exposure to the acidic solution. Subsequently, the external pH was shifted to pH 8. As a result, the internal pH in the cell coexpressing the M2 channel changes quickly, while a much slower pH change was observed in the cell that does not express M2. After 6 min, both cells exhibit a similar pH (see Fig. 10), and after 10 min the M2-expressing cell reached pH 8 and showed even a slightly higher pH than the cell expressing eGFP-pHsens only (without M2). The color plots shown at the right side of Fig. 10 (2 min–10 min) resemble the internal pH change only, while the color for the external environment is kept in blue without correlation to the pH for better visibility.

As mentioned above, amantadine binds to the M2 channel and blocks the influx of protons. To test the effect of amantadine, the intracellular pH change after adding amantadine at a final concentration of 100 μM was measured. Fig. 11 shows the time course of the pH change in CHO-K1 cells expressing eGFP-pHsens and M2-TagRFP without (black squares) and with amantadine (blue triangles) in the buffer. In comparison, the effect of the same shift in extracellular pH on

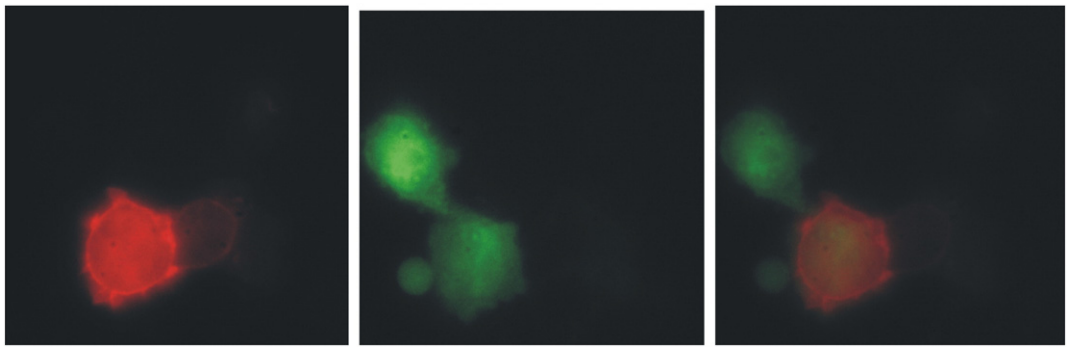

Fig. 9. CHO-K1 cells transfected with M2-TagRFP shown in red (left panel) and the pH-sensitive eGFP-pHsens shown in green (middle panel). One of the two cells shown expresses both transfected proteins (eGFP-pHsens and the fusion protein M2-TagRFP) while the other cell only expresses eGFP-pHsens. The right panel displays the overlay of the first 2 panels.

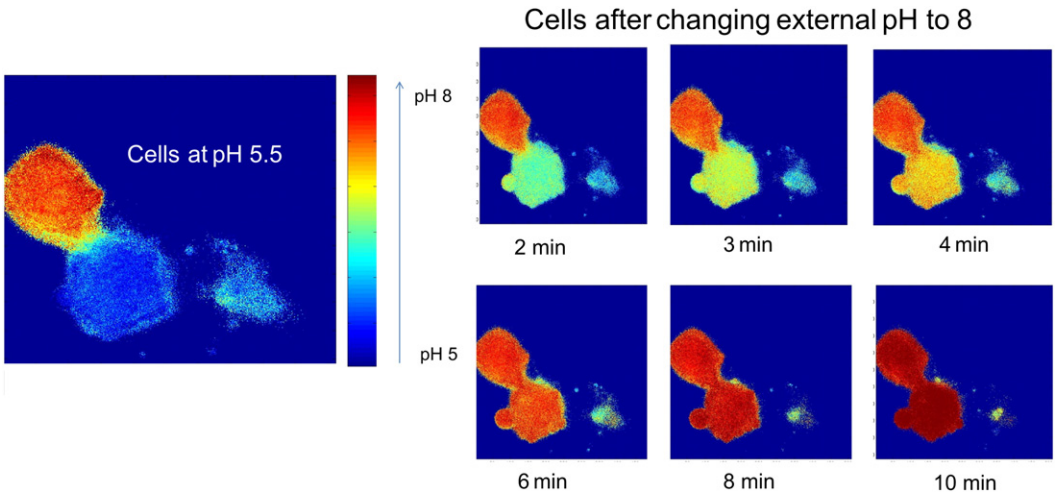

Fig. 10. pH changes shown as color plot measured in the two cells displayed in Fig. 9. The pH is encoded by a chromatic color scheme, see left panel.

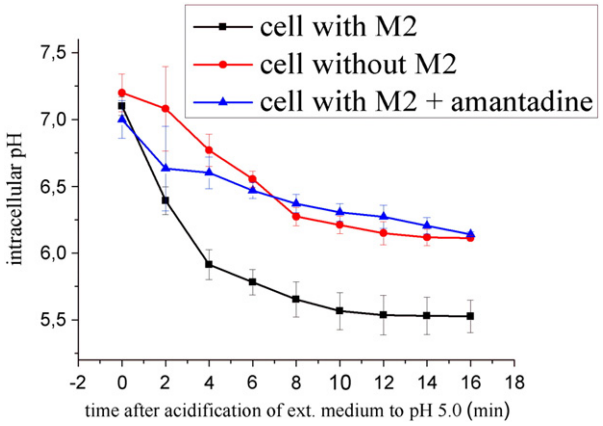

Fig. 11. pH in CHO-K1 cells expressing M2 channels without (black squares) and with amantadine (blue triangles) in comparison to control cells not expressing M2 (red circles).

intracellular pH is shown from control cells only expressing eGFP-pHsens, but not the proton channel (red circles in Fig. 11). The confidence intervals indicate the standard deviation of four different measurements for each cell type. The pH change in cells with M2 channels (black squares in Fig. 11) shows a fast decrease upon acidification of the external medium to pH 5. After about 10 min, the internal pH saturates at about pH 5.5. Cells which do not express M2 clearly exhibit a slower and less profound pH change (red circles in Fig. 11). They also exhibit a retarded response of the intracellular pH after changing the external solution to pH 5, and the time course does not seem to be exponential. Upon incubation of M2-expressing cells with 100 μM amantadine in the PBSeq buffer (pH 5) a behavior similar to control cells devoid of M2 channels was observed (blue triangles in Fig. 11 in comparison to the red circles, respectively). Within the confidence interval, the behavior of the cells expressing M2 upon blocking by amantadine and the behavior of the cells without M2 (control) are comparable. These experiments show that the expression of M2 in mammalian cells leads to a M2-specific, drastic augmentation of proton transport across the cell membrane. The specificity of the pH response can be seen from the fact that proton uptake is reduced to background level in the presence of the M2-specific blocker amantadine.

Another feature of the FLIM technique applied to eGFP-pHsens is the possibility to monitor the pH not only in the cytoplasm but also in intracellular organelles like mitochondria or chloroplasts, still with high sensitivity and good contrast just by expression of eGFP-pHsens as a fusion protein with mitochondrial targeting sequences. In general, the simultaneous determination of pH in the cytosol and small cellular compartments by external pH indicator dyes is difficult since the applied dye may or may not be suitable to selectively reach the desired cell compartments such as mitochondria. In contrast, the genetically encoded fluorescence proteins can confidently be targeted to the sub-cellular structure of interest. Therefore, additional chemical properties that allow for the penetration across cellular membranes do not necessarily have to be considered. The specific design of the fluorescence proteins with a suitable targeting sequence ensures organelle-selective staining. We demonstrate such an application for simultaneous pH measurement in the cytosol and mitochondria of CHO-K1 cells cotransfected with eGFP-pHsens (expressed in the cytoplasm) and eGFP-pHsens targeted to mitochondria in Fig. 12. As shown in Fig. 12, the cells exhibit clearly distinguishable fluorescence from the cytoplasm and the mitochondria, which appear slightly brighter than the cell cytoplasm in the intensity picture (measured with the MA detector) depicted in Fig. 12, right side. Closer inspection of the FLIM pictures (see Fig. 12, left side) reveals that the pH in the mitochondria is slightly higher (around 7.8) than the pH in the cytoplasm (about 7.0).

4. Model-based analysis of the pH change in CHO-K1 cells

The observed pH dynamics as shown in Fig. 11 can be modeled by an apparent diffusion process of protons across the cell membrane that is subsuming the effects that contribute to a net change of the pH concentration in the cell cytosol. Starting from the free diffusion equation that equals the continuity equation for a free particle stream for the time derivative of the time dependent concentration $c(t)$ inside the cell with the "apparent diffusion" constant D

$$\dot{c}(t) = D\Delta c(t) \tag{3}$$

one can derive a simplification for the Laplacian of the concentration $\Delta c(t)$, i.e. the second spatial derivative of the concentration across the cell membrane in the form of the difference between the internal concentration $c_i(t)$ and the constant external concentration c_A divided by the square of the membrane thickness Δx:

$$\Delta c(t) = \frac{c_i(t) - c_A}{\Delta x^2} = \frac{1}{D}\dot{c}_i(t). \tag{4}$$

From that simplification one achieves the general expression $c_i(t) = Ae^{-\frac{D}{\Delta x^2}t} + K$ with the constants A and K.

K determines the equilibrium pH in the cell $K = c_{eq.}$ and A is determined by the boundary condition $c_i^0 - c_{eq.} = A$ with the initial pH in the cytoplasm c_i^0:

$$c_i(t) = \left(c_i^0 - c_{eq.}\right)e^{-\frac{D}{\Delta x^2}t} + c_{eq.}. \tag{5}$$

Eq. (5) directly delivers the time dependent pH inside the cell lumen as

$$\mathrm{pH}(t) = -\log(c_i(t)) = -\log\left[\left(c_i^0 - c_{eq.}\right)e^{-\frac{D}{\Delta x^2}t} + c_{eq.}\right]. \tag{6}$$

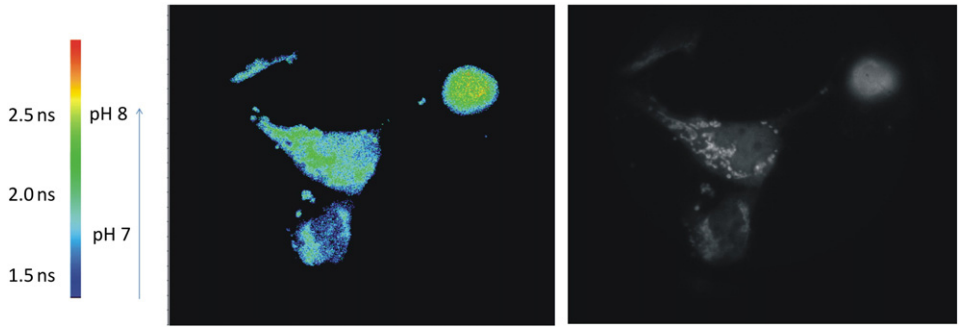

Fig. 12. FLIM images of CHO-K1 cells expressing eGFP-pHsens in the cytoplasm and additionally cotransfected with eGFP-pHsens targeted to mitochondria. The fluorescence intensity picture is shown at the right side. The corresponding fluorescence lifetime distribution is shown in the chromatic scale as depicted on the left side.

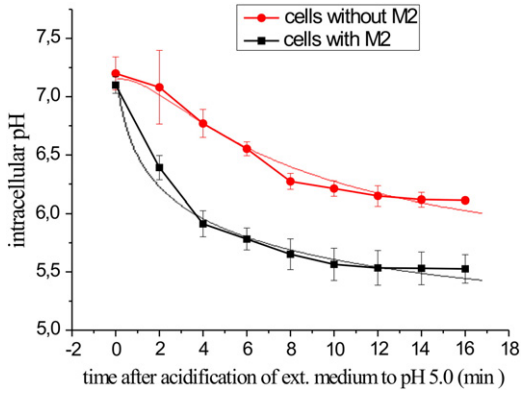

Fig. 13. Comparison of the diffusion model as described by Eqs. (6) and (7) with the corresponding behavior of cells with (red) and without (black) M2 channels as shown in Fig. 11. The red solid line indicates the fit with constant diffusion coefficient (Eq. (6)) and the black solid line with time dependent diffusion coefficient (Eq. (7)).

For a given thickness of the cell membrane Eq. (6) contains two free parameters, the "diffusion coefficient" D and the equilibrium proton concentration $c_{eq.}$. As shown in Fig. 11, the pH seems to decay exponentially in time after acidification of the external lumen (black squares in Figs. 11, 13).

Fig. 13 displays the result after fitting the formula (6) to the measurement data (black solid line in comparison to black squares) starting at pH(t=0) = 7.1 $\left(c_i{}^0 = 7.9 \cdot 10^{-8}\ \text{mol/l}\right)$ with $\frac{D}{\Delta x^2} = 6.7 \cdot 10^{-4}\ \text{s}^{-1}$ and pH(eq.) = 5.1 ($c_{eq.} = 7.9 \cdot 10^{-6}$ mol/l).

Assuming that the cell membrane has a physical thickness of 10 nm the resulting diffusion coefficient (D) is $D = 6.7 \cdot 10^{-16}$ cm ²/s.

For the control cells not expressing M2, the temporal change of the pH (red circles in Fig. 13) cannot be fit by Eq. (6). Instead of the purely exponential behavior one has to assume that D is time-dependent.

The red solid line in Fig. 13 represents a fit with

$$\frac{D}{\Delta x^2} = 6.7 \cdot 10^{-4}\ \text{s}^{-1} \cdot \left(1 - \exp\left(-1.8 \cdot 10^{-3}\ \text{s}^{-1} \cdot t\right)\right). \quad (7)$$

In addition, a slightly higher starting pH(t=0) of 7.15 $\left(c_i{}^0 = 7.1 \cdot 10^{-8}\ \text{mol/l}\right)$ and a clearly higher pH(eq.) = 5.6 ($c_{eq.}$= 2.5 · 10^{-6} mol/l) had to be assumed.

However, typical values for the diffusion of protons inside the cytoplasm are determined to be 10^{-6} cm^2/s [71] with values of 5.8 10^{-5} cm^2/s determined for the transversal diffusion of protons across lipid bilayers [72] due to the fast transfer of protons along acidic groups in the lipid membrane.

This simplified analysis shows that the step of the protons crossing the membrane cannot be the rate-limiting step determining the pH kinetics in the cytosol after acidification of the surrounding medium, since the values for the transversal diffusion coefficient found in the literature differ from the observed pH kinetics by 10 orders of magnitude. The determining parameters for the pH change are therefore the general permeability of the cell membrane for protons, buffer capacity inside the cell and/or active outwardly directed proton pumping. In addition, the permeability of the M2 channel itself is pH-dependent [73]. This would also account for acid carriers as proposed as fast proton transporters in the cell membrane [71]. Active outwardly directed proton pumping and downregulation of proton carriers at low pH determine the equilibrium proton concentration $c_{eq.}$ that is reached after sufficiently long time in the acidified medium. The results of Fig. 13 clearly show that the number of protons crossing the cell membrane is much higher in cells containing M2 than in cells without proton channels as one would expect from the assumed function of M2 as an active proton transporter.

5. Discussion

In this study, we show how eGFP-pHsens can be used for a targeted measurement of the local pH in living cells and small cell organelles by fluorescence lifetime determination. The technique provides a tool to analyze selectively proton transfer processes across cellular membranes and into small intracellular organelles.

Compared to ratiometric pH measurement techniques with fluorescent dyes, which evaluate only the total intensity of the fluorescence in certain spectral regions, the pH determination based on the fluorescence lifetime by FLIM provides several decisive advantages: Firstly, the influence of cellular autofluorescence or fluorescent contaminants can be separated by measuring the fluorescence lifetime and evaluating the contribution of characteristic fluorescence decay times of the eGFP-pHsens protein. The fluorescence lifetime is also independent from the actual fluorophore concentration (which depends on the expression level). Secondly, in contrast to ratiometric techniques, FLIM allows the pH determination by measuring one wavelength section around 520 nm only. The FLIM method allows a highly sensitive pH measurement, with in principle only diffraction-limited spatial resolution. The implementation of novel, high-resolution methods even allows gaining information from structures that are smaller than the diffraction limit. This especially accounts for the application of photoswitchable fluorescence proteins. An additional application of eGFP-pHsens could be the use as a highly efficient, pH-dependent photoswitch. Thirdly, organelle-specific targeting sequences can be used allowing for the design of target-specific assays for all proton transporting membrane proteins of interest in pharmacology. Due to the robustness and sensitivity and the recent development of high-throughput FLIM detectors based on the single photon counting technique, the assay can easily be parallelized (e.g. adaptation to a common microtiter plate format for high-throughput screening).

The model based analysis of the pH dynamics in CHO-K1 cells revealed that the apparent diffusion constant is not determined by the process of transversal diffusion over the cell membrane. The retarded pH adaption as observed in cells not expressing M2 (red curve in Fig. 13) strongly indicates that proton 'sinks' exist inside the cell lumen that buffer protons until the internal pH starts to change. This allows for the quantitative analysis of the buffer capacity of the cell lumen. The buffer capacity can also explain the deviation between the black measured squares and the solid fit (black line) in Fig. 13 observed in the short time regime at 2 min after acidification of the external medium.

After 10–12 min, it is evident that the intracellular pH in M2-expressing cells equilibrates on a higher value in comaprison to cells not expressing M2. This difference can be explained by a flux of protons that are actively pumped out of the cell, which prevents the cytoplasm to reach equilibrium with the external acidic medium. In conclusion, the observed pH dynamics (Figs. 11 and 13) denotes the pathway from a strong pH gradient between the cytoplasm and the external lumen to an equilibrium that is determined by the H^+ permeability of the cell membrane, active proton pumps that reduce the internal proton concentration and strongly pH-dependent proton carriers. The time constants of Eqs. (6) and (7) denote the kinetics from the initial pH gradient to the equilibrium for M2 containing cells and cells not containing M2, respectively. The deviation of the shape of the fit curve in Fig. 13 from the exponential one is mainly determined by the buffer capacity of the cell cytoplasm. Finally, the equilibrium pH is a ruler for the pH dependency of proton carriers and the activity of active proton pumping in comparison to the number of protons that can cross the cell membrane along the gradient. Proton transporters might be acid carriers localized in the cell membrane as proposed by [71].

6. Conclusions and future perspectives for photosynthesis research

The proposed technique to employ eGFP-pHsens in a FLIM-based setup is suitable for large scale automated screening of compound libraries to identify drugs directed against influenza A virus by

specifically blocking the M2 proton channel, similar to the mode of action of amantadine. The applicability of GFP based fluorophores suitable for biomedical imaging will be strongly expanded in future research including the quantitative analyses of chromophore to protein matrix interactions, chromophore to membrane protein interactions, chromophore–chromophore interactions and light-induced dynamic processes. It is a promising approach to expand the technique to pharmaceutical drug research regarding other proton transporters like the gastric H^+/K^+-ATPase. This protein plays an important role in the treatment of gastric ulcers or in the therapy of infections with *Helicobacter pylori* [57,74]. With eGFP-pHsens, stable cell lines that are grown on microwell plates and function as a high-throughput test system that can be quickly and precisely scanned by evaluating the fluorescence decay time of the fluorescence protein could be generated. Such devices can be used to identify drugs blocking proton-translocating membrane proteins in general, and in particular compounds acting against the M2 channel are still valuable research targets [75]. Since the influenza A virus mutates quickly, with the M2 coding sequence being particularly prone to mutations, these viruses can be selectively scanned for such mutations and used for targeted drug development against the structurally changed M2 proteins of resistant influenza A strains. This includes the test for possible resistance against amantadine. This approach does count not only for the influenza A virus, but for all virus particles containing proton channels in order to facilitate the directed design of channel inhibitors.

Functionalized GFP based sensors are suitable to monitor metabolic processes including sensors for reactive oxygen species (ROS), Ca^{2+}, NAD^+/NAHD and pH (see [35] for a list of available sensor proteins). Although most applications have been reported in animal cells, the broad range of available genetically encoded fluorescent chemosensors can as well be applied in plants. Special applications related to the determination of pH in cell walls and in the cytosol with the highest spatial resolution have already been suggested [76,77]. Precise organelle-specific determination of pH offers promising perspectives for future photosynthesis research. Following the time course of ΔpH generation across thylakoid membranes would allow for a correlation of ΔpH evolution with the kinetics of the development of the qE component of NPQ processes including the xanthophyll contributions. Correlation of pH sensing with probes specific for certain ROS might be able to disentangle the interplay between the two systems. Furthermore, applications of pH-sensing fluorescence proteins that are tagged to the luminal side of the WOC in PSII would enable the detection of proton release events that are difficult to determine since the autofluorescence of the Chl molecules is much stronger than that of animal cells, which do not contain such an abundance of intrinsic chromophores. Therefore, the chromophores having a design that can be excited in the green spectral range with characteristic fluorescence lifetime are the most promising candidates for in vivo plant spectroscopy employing genetically-encoded fluorescence proteins [78]. The proposed technique can be used to investigate "proton pumps, such as cytochrome c oxidase (CcO), [which] translocate protons across biological membranes at a rate that considerably exceeds the rate of proton transport to the entrance of the proton-conducting channel via bulk diffusion" [79].

For application of GFP-based chemosensors in photosynthesis research, the main problem of the overlapping Chl fluorescence has to be considered seriously. Whereas the excitation spectrum of GFP itself significantly overlaps with Chl excitation, the spectral properties of the yellow fluorescent protein (YFP) would be better suited, since it can be excited in the green at 520 nm. Therefore, future developments of chemosensors for plant cell research should better focus on YFP as a template to achieve robust applicability in photosynthetic organisms. Of note, high-resolution FLIM not only allows for the simultaneous analysis of fluorescence intensity in different wavelength sections and fluorescence lifetimes with high spatial resolution, but it can also add additional parameters like fluorescence polarization/anisotropy and is applicable in several microscopic modes including confocal laser scanning, wide field illumination, fluorescence recovery after photobleaching and fluorescence correlation spectroscopy (see also [68]).

Acknowledgements

The authors are grateful for the support by the Federal Ministry of Education and Research (BMBF, project Quantum, FKZ 13N10067 and BMBF-RUS 11/014) and the German Research Foundation (Deutsche Forschungsgemeinschaft, Cluster of Excellence "Unifying Concepts in Catalysis") and to the Leibniz Institute for Neurobiology (IfN) in Magdeburg (Germany) for generously granting us the novel MA TSCSPC detector. T. Friedrich and F.-J. Schmitt acknowledge COST for the support in the framework of COST action MP1205. B. Thaa and M. Veit thank the German Research Foundation for financial support in the framework of SfB 740. We thank Dr. W. Zuschratter (IfN Magdeburg) for providing the TagRFP-T cDNA clone and Ina Seuffert for technical assistance.

References

[1] G.T. Hanson, T.B. McAnaney, E.S. Park, M.E. Rendell, D.K. Yarbrough, S. Chu, L. Xi, S.G. Boxer, M.H. Montrose, S.J. Remington, Green fluorescent protein variants as ratiometric dual emission pH sensors. 1. Structural characterization and preliminary application, Biochemistry 41 (2002) 15477–15488.
[2] B. Genty, J.M. Briantais, N.R. Baker, The relationship between the quantum yield of photosynthetic electron transport and quenching of chlorophyll fluorescence, Biochim. Biophys. Acta 990 (1989) 87–92.
[3] K. Roháček, Chlorophyll fluorescence parameters: the definitions, photosynthetic meaning, and mutual relationships, Photosynthetica 40 (2002) 13–29.
[4] A. Stirbet, Govindjee, On the relation between the Kautsky effect (chlorophyll a fluorescence induction) and Photosystem II: basics and applications of the OJIP fluorescence transient, J. Photochem. Photobiol. B 104 (2011) 236–257.
[5] W. Bigler, U. Schreiber, Chlorophyll luminescence as an indicator of stress-induced damage to the photosynthetic apparatus. Effects of heat-stress in isolated chloroplasts, Photosynth. Res. 25 (1990) 161–171.
[6] V. Goltsev, I. Zaharieva, P. Chernev, R.J. Strasser, Delayed fluorescence in photosynthesis, Photosynth. Res. 101 (2009) 217–232.
[7] P. Lambrev, V. Goltsev, pH dependence of the effects of diuron, atrazine and dinoseb on the luminescent properties of thylakoid membranes, Bulg. J. Plant Physiol. (2001) 85–100.
[8] F.-J. Schmitt, Picobiophotonics for the Investigation of Pigment–Pigment and Pigment–Protein Interactions in Photosynthetic Complexes, (in: PhD thesis, Department of Physics, Technical University of Berlin, Berlin) 2011.
[9] D.M. Kramer, A.R. Crofts, Control of photosynthesis and measurement of photosynthetic reactions in intact plants, in: N.R. Baker (Ed.), Photosynthesis and the Environment, Advances in PhotosynthesisKluiver Academic Press, Dordrecht, 1996, pp. 25–66.
[10] H.-J. Eckert, G. Renger, Temperature dependence of $P680^+$ reduction in O_2-evolving PS II membrane fragments at different redox states S_i of the water oxidizing system, FEBS Lett. 236 (1988) 425–431.
[11] G. Renger, Oxidative photosynthetic water splitting: energetics, kinetics and mechanism, Photosynth. Res. 92 (2007) 407–425.
[12] G. Renger, Role of hydrogen bonds in photosynthetic water splitting, in: K.-L. Han, G.J. Zhao (Eds.), Excited State Hydrogen Bonding and Hydrogen Transfer, Wiley, Chichester, 2010, pp. 433–461.
[13] G. Renger, Light induced oxidative water splitting in photosynthesis: energetics, kinetics and mechanism, J. Photochem. Photobiol. B 104 (2011) 35–43.
[14] G. Renger, Mechanism of light induced water splitting in Photosystem II of oxygen evolving photosynthetic organisms, Biochim. Biophys. Acta 1817 (2012) 1164–1176.
[15] P. Mitchell, Coupling of phosphorylation to electron and hydrogen transfer by a chemi-osmotic type of mechanism, Nature 191 (1961) 144–148.
[16] W. Junge, H. Lill, S. Engelbrecht, ATP synthase: an electrochemical transducer with rotatory mechanics, Trends Biochem. Sci. 22 (1997) 420–423.
[17] P. Horton, M.P. Johnson, M.L. Perez-Bueno, A.Z. Kiss, A.V. Ruban, Photosynthetic acclimation: does the dynamic structure and macro-organisation of photosystem II in higher plant grana membranes regulate light harvesting states? FEBS J. 275 (2008) 1069–1079.
[18] H. Härtel, H. Lokstein, B. Grimm, B. Rank, Kinetic studies on the xanthophyll cycle in barley leaves (influence of antenna size and relations to nonphotochemical chlorophyll fluorescence quenching), Plant Physiol. 110 (1996) 471–482.
[19] B. Demmig-Adams, A.M. Gilmore, W.W. Adams III, The role of the xanthophyll cycle carotenoids in the protection of photosynthesis, Trends Plant Sci. 1 (1996) 21–26.
[20] M.P. Johnson, P.A. Davison, A.V. Ruban, P. Horton, The xanthophyll cycle pool size controls the kinetics of non-photochemical quenching in *Arabidopsis thaliana*, FEBS Lett. 582 (2008) 262–266.
[21] M.P. Johnson, M.L. Perez-Bueno, A. Zia, P. Horton, A.V. Ruban, The zeaxanthin-independent and zeaxanthin-dependent qE components of nonphotochemical quenching involve common conformational changes within the photosystem II antenna in *Arabidopsis*, Plant Physiol. 149 (2009) 1061–1075.
[22] S. Crouchman, A. Ruban, P. Horton, PsbS enhances nonphotochemical fluorescence quenching in the absence of zeaxanthin, FEBS Lett. 580 (2006) 2053–2058.

[23] A.Z. Kiss, A.V. Ruban, P. Horton, The PsbS protein controls the organization of the photosystem II antenna in higher plant thylakoid membranes, J. Biol. Chem. 283 (2008) 3972–3978.
[24] K.K. Niyogi, T.B. Truong, Evolution of flexible non-photochemical quenching mechanisms that regulate light harvesting in oxygenic photosynthesis, Curr. Opin. Plant Biol. 16 (2013) 307–314.
[25] P. Müller, X.P. Li, K.K. Niyogi, Non-photochemical quenching. A response to excess light energy, Plant Physiol. 125 (2001) 1558–1566.
[26] I. Szabo, E. Bergantino, G.M. Giacometti, Light and oxygenic photosynthesis: energy dissipation as a protection mechanism against photo-oxidation, EMBO Rep. 6 (2005) 629–634.
[27] E. Bergantino, A. Segalla, A. Brunetta, E. Teardo, F. Rigoni, G.M. Giacometti, I. Szabo, Light- and pH-dependent structural changes in the PsbS subunit of photosystem II, Proc. Natl. Acad. Sci. U. S. A. 100 (2003) 15265–15270.
[28] T.K. Goral, M.P. Johnson, C.D. Duffy, A.P. Brain, A.V. Ruban, C.W. Mullineaux, Light-harvesting antenna composition controls the macrostructure and dynamics of thylakoid membranes in *Arabidopsis*, Plant J. 69 (2012) 289–301.
[29] H.A. Frank, A. Cua, V. Chynwat, A. Young, D. Gosztola, M.R. Wasielewski, Photophysics of the carotenoids associated with the xanthophyll cycle in photosynthesis, Photosynth. Res. 41 (1994) 389–395.
[30] Y.Z. Ma, N.E. Holt, X.P. Li, K.K. Niyogi, G.R. Fleming, Evidence for direct carotenoid involvement in the regulation of photosynthetic light harvesting, Proc. Natl. Acad. Sci. U. S. A. 100 (2003) 4377–4382.
[31] R. Desikan, S.A.-H. Mackerness, J.T. Hancock, S.J. Neill, Regulation of the *Arabidopsis* transcriptome by oxidative stress, Plant Physiol. 127 (2001) 159–172.
[32] C.H. Foyer, S. Shigeoka, Understanding oxidative stress and antioxidant functions to enhance photosynthesis, Plant Physiol. 155 (2011) 93–100.
[33] A. Krieger-Liszkay, Singlet oxygen production in photosynthesis, J. Exp. Bot. 56 (2005) 337–346.
[34] R. Mittler, S. Vanderauwera, N. Suzuki, G. Miller, V.B. Tognetti, K. Vandepoele, M. Gollery, V. Shulaev, F. Van Breusegem, ROS signaling: the new wave? Trends Plant Sci. 16 (2011) 300–309.
[35] F.J. Schmitt, G. Renger, T. Friedrich, V.D. Kreslavski, S.K. Zharmukhamedov, D.A. Los, V.V. Kuznetsov, S.I. Allakhverdiev, Reactive oxygen species: re-evaluation of generation, monitoring and role in stress-signaling in phototrophic organisms, Biochim. Biophys. Acta 1837 (2014) 835–848.
[36] R.E. Slovacek, G. Hind, Energetic factors affecting carbon dioxide fixation in isolated chloroplasts, Plant Physiol. 65 (1980) 526–532.
[37] J. Crofts, P. Horton, Dissipation of excitation energy by Photosystem II particles at low pH, Biochim. Biophys. Acta 1058 (1991) 187–193.
[38] R. Heim, D.C. Prasher, R.Y. Tsien, Wavelength mutations and posttranslational autoxidation of green fluorescent protein, Proc. Natl. Acad. Sci. USA 91 (1994) 12501–12504.
[39] G.J. Kremers, S.G. Gilbert, P.J. Cranfill, M.W. Davidson, D.W. Piston, Fluorescent proteins at a glance, J. Cell Sci. 124 (2011) 157–160.
[40] O. Shimomura, F.H. Johnson, Y. Saiga, Extraction, purification and properties of aequorin, a bioluminescent protein from the luminous hydromedusan, *Aequorea*, J. Cell. Comp. Physiol. 59 (1962) 223–239.
[41] F. Yang, L.G. Moss, G.N. Phillips Jr., The molecular structure of green fluorescent protein, Nat. Biotechnol. 14 (1996) 1246–1251.
[42] W.W. Ward, H.J. Prentice, A.F. Roth, C.W. Cody, S.C. Reeves, Spectral perturbations of the *Aequorea* green-fluorescent protein, Photochem. Photobiol. 35 (1982) 803–808.
[43] G. Miesenböck, D.A. De Angelis, J.E. Rothman, Visualizing secretion and synaptic transmission with pH-sensitive green fluorescent proteins, Nature 394 (1998) 192–195.
[44] M. Zimmer, Green fluorescent protein (GFP): applications, structure, and related photophysical behavior, Chem. Rev. 102 (2002) 759–781.
[45] R. Heim, A.B. Cubitt, R.Y. Tsien, Improved green fluorescence, Nature 373 (1995) 663–664.
[46] M. Kneen, J. Farinas, Y. Li, A.S. Verkman, Green fluorescent protein as a noninvasive intracellular pH indicator, Biophys. J. 74 (1998) 1591–1599.
[47] M. Di Donato, L.J. van Wilderen, I.H. Van Stokkum, T.C. Stuart, J.T. Kennis, K.J. Hellingwerf, R. van Grondelle, M.L. Groot, Proton transfer events in GFP, Phys. Chem. Chem. Phys. 13 (2011) 16295–16305.
[48] R. Bizzarri, M. Serresi, S. Luin, F. Beltram, Green fluorescent protein based pH indicators for in vivo use: a review, Anal. Bioanal. Chem. 393 (2009) 1107–1122.
[49] T.N. Campbell, F.Y.M. Choy, The effect of pH on green fluorescent protein: a brief review, Mol. Biol. Today 2 (2001) 1–4.
[50] J. Llopis, J.M. McCaffery, A. Miyawaki, M.G. Farquhar, R.Y. Tsien, Measurement of cytosolic, mitochondrial, and Golgi pH in single living cells with green fluorescent proteins, Proc. Natl. Acad. Sci. U. S. A. 95 (1998) 6803–6808.
[51] S. Sankaranarayanan, D. De Angelis, J.E. Rothman, T.A. Ryan, The use of pHluorins for optical measurements of presynaptic activity, Biophys. J. 79 (2000) 2199–2208.
[52] R.M. Wachter, B.A. King, R. Heim, K. Kallio, R.Y. Tsien, S.G. Boxer, S.J. Remington, Crystal structure and photodynamic behavior of the blue emission variant Y66H/Y145F of green fluorescent protein, Biochemistry 36 (1997) 9759–9765.
[53] A. Chevrollier, D. Loiseau, B. Chabi, G. Renier, O. Douay, Y. Malthiery, G. Stepien, ANT2 isoform required for cancer cell glycolysis, J. Bioenerg. Biomembr. 37 (2005) 307–316.
[54] D. Nelson, M. Cox, A. Held, Lehninger: Principles of Biochemistry, 5th ed. W.H. Freeman and Company, New York, 2008.
[55] T.N. Seyfried, Cancer as a Metabolic Disease, Wiley, New Jersey, 2012.
[56] J.M. Weinberg, M.A. Venkatachalam, N.F. Roeser, I. Nissim, Mitochondrial dysfunction during hypoxia/reoxygenation and its correction by anaerobic metabolism of citric acid cycle intermediates, Proc. Natl. Acad. Sci. U. S. A. 97 (2000) 2826–2831.
[57] G. Sachs, J.M. Shin, O. Vagin, N. Lambrecht, I. Yakubov, K. Munson, The gastric H, K ATPase as a drug target: past, present, and future, J. Clin. Gastroenterol. 41 (Suppl. 2) (2007) S226–S242.
[58] J.M. Shin, K. Munson, O. Vagin, G. Sachs, The gastric HK-ATPase: structure, function, and inhibition, Pflugers Arch. 457 (2009) 609–622.
[59] S. Hamamah, J.L. Gatti, Role of the ionic environment and internal pH on sperm activity, Hum. Reprod. 13 (Suppl. 4) (1998) 20–30.
[60] L.H. Pinto, R.A. Lamb, The M2 proton channels of influenza A and B viruses, J. Biol. Chem. 281 (2006) 8997–9000.
[61] I.V. Chizhmakov, F.M. Geraghty, D.C. Ogden, A. Hayhurst, M. Antoniou, A.J. Hay, Selective proton permeability and pH regulation of the influenza virus M2 channel expressed in mouse erythroleukaemia cells, J. Physiol. 494 (Pt 2) (1996) 329–336.
[62] A.J. Hay, A.J. Wolstenholme, J.J. Skehel, M.H. Smith, The molecular basis of the specific anti-influenza action of amantadine, EMBO J. 4 (1985) 3021–3024.
[63] X. Jing, C. Ma, Y. Ohigashi, F.A. Oliveira, T.S. Jardetzky, L.H. Pinto, R.A. Lamb, Functional studies indicate amantadine binds to the pore of the influenza A virus M2 proton-selective ion channel, Proc. Natl. Acad. Sci. U. S. A. 105 (2008) 10967–10972.
[64] J.A. Mould, J.E. Drury, S.M. Frings, U.B. Kaupp, A. Pekosz, R.A. Lamb, L.H. Pinto, Permeation and activation of the M2 ion channel of influenza A virus, J. Biol. Chem. 275 (2000) 31038–31050.
[65] K. Shimbo, D.L. Brassard, R.A. Lamb, L.H. Pinto, Ion selectivity and activation of the M2 ion channel of influenza virus, Biophys. J. 70 (1996) 1335–1346.
[66] S.H. Shim, C. Xia, G. Zhong, H.P. Babcock, J.C. Vaughan, B. Huang, X. Wang, C. Xu, G.Q. Bi, X. Zhuang, Super-resolution fluorescence imaging of organelles in live cells with photoswitchable membrane probes, Proc. Natl. Acad. Sci. U. S. A. 109 (2008) 13978–13983.
[67] H.J. Lin, P. Herman, J.R. Lakowicz, Fluorescence lifetime-resolved pH imaging of living cells, Cytometry A 52 (2003) 77–89.
[68] F.J. Schmitt, E.G. Maksimov, C. Junghans, J. Weißenborn, P. Hätti, V.Z. Paschenko, S.I. Allakhverdiev, T. Friedrich, Structural organization and dynamic processes in protein complexes determined by multiparameter imaging, NanoPhotoBiosciences 1 (2013) 1–45.
[69] F.J. Schmitt, E.G. Maksimov, P. Hatti, J. Weissenborn, V. Jeyasangar, A.P. Razjivin, V.Z. Paschenko, T. Friedrich, G. Renger, Coupling of different isolated photosynthetic light harvesting complexes and CdSe/ZnS nanocrystals via Förster resonance energy transfer, Biochim. Biophys. Acta 1817 (2012) 1461–1470.
[70] Becker&Hickl_GmbH, PML-16-C 16 Channel Detector Head for Time-Correlated Single Photon Counting User Handbook, Becker & Hickl GmbH, Berlin, 2006.
[71] N.F. al-Baldawi, R.F. Abercrombie, Cytoplasmic hydrogen ion diffusion coefficient, Biophys. J. 61 (1992) 1470–1479.
[72] S. Serowy, S.M. Saparov, Y.N. Antonenko, W. Kozlovsky, V. Hagen, P. Pohl, Structural proton diffusion along lipid bilayers, Biophys. J. 84 (2003) 1031–1037.
[73] T. Leiding, J. Wang, J. Martinsson, W.F. DeGrado, S.P. Arskold, Proton and cation transport activity of the M2 proton channel from influenza A virus, Proc. Natl. Acad. Sci. U. S. A. 107 (2010) 15409–15414.
[74] G. Sachs, D.R. Scott, Y. Wen, Gastric infection by *Helicobacter pylori*, Curr. Gastroenterol. Rep. 13 (2011) 540–546.
[75] A.D. Balgi, J. Wang, D.Y. Cheng, C. Ma, T.A. Pfeifer, Y. Shimizu, H.J. Anderson, L.H. Pinto, R.A. Lamb, W.F. DeGrado, M. Roberge, Inhibitors of the influenza A virus M2 proton channel discovered using a high-throughput yeast growth restoration assay, PLoS One 8 (2013) e55271.
[76] W.G. Choi, S.J. Swanson, S. Gilroy, High-resolution imaging of Ca^{2+}, redox status, ROS and pH using GFP biosensors, Plant J. 70 (2012) 118–128.
[77] S.J. Swanson, W.G. Choi, A. Chanoca, S. Gilroy, In vivo imaging of Ca^{2+}, pH, and reactive oxygen species using fluorescent probes in plants, Annu. Rev. Plant Biol. 62 (2011) 273–297.
[78] K. Kobayashi, T. Matsuda, Spatial and Temporal regulation of chloroplast development in *Arabidopsis* root, Photosynthesis Research for Food, Fuel and the Future, Springer, Berlin, 2013, pp. 389–393.
[79] Y. Georgievskii, E.S. Medvedev, A.A. Stuchebrukhov, Proton transport via the membrane surface, Biophys. J. 82 (2002) 2833–2846.